Appendix (Supplementary Methods and Results) of

Contribution of Ictal Source Imaging for localizing Seizure Onset Zone in Patients with Focal Epilepsy Patients

Shuai Ye, M.S.[1,*], Lin Yang, Ph.D.[2,*], Yunfeng Lu, Ph.D.[2], Michal T. Kucewicz, Ph.D.[3], Benjamin Brinkmann, Ph.D.[3], Cindy Nelson, R. EEG T.[3], Abbas Sohrabpour, Ph.D.[1], Gregory A. Worrell, M.D., Ph.D.[3], Bin He, Ph.D.[1,#]

[1] Department of Biomedical Engineering, Carnegie Mellon University, Pittsburgh, PA;

[2] Department of Biomedical Engineering, University of Minnesota, Minneapolis, MN;

[3] Mayo Clinic, Rochester, MN

* Contributed equally

Correspondence: bhe1@andrew.cmu.edu

TABLE OF CONTENTS

INTRODUCTION

Scalp EEG is currently the only established non-invasive electrophysiological mapping tool that provides reliable seizure recording for the pre-surgical evaluation of epilepsy. The aim of the present study is to evaluate the clinical applicability of a non-invasive seizure imaging approach, which bridges the scalp sensors and underlying epilepsy sources. The study is divided into two parts:

In the ictal activity study, we aim to evaluate the performance and merits of recording and dynamically imaging seizure sources from high-density scalp EEG. A comprehensive pipeline involving the integration of various information is employed to validate the accuracy of ictal activity analysis.

In the interictal activity study, we aim to evaluate the challenges posed when performing the classical interictal activity analysis. By comparing the results from ictal analysis and interictal analysis, we aim to show the added value of ictal source analysis in clinical setting.

MATERIALS AND METHODS

Patient Number Breakdown and Clarification

In 20 patients out of the 39 patients, iEEG recordings were available, i.e. electrode placement could be confirmed from available CT images, and 34 patients had surgical resection (in 28 of these patients, post-op MRI was available). In the 20 patients with iEEG recordings, 15 had surgery, and post-op MRI was available in 9 of these patients (out of 15), from which the resected volume was extracted. The patient number breakdown is schematically depicted in (Fig. S1).

It is important to note that, in clinical practice, one patient may not undergo both iEEG monitoring and surgical resection. For example, some patients might undergo surgery without the need for any prior iEEG monitoring, and some patients who undergo iEEG monitoring, might be offered other treatments, such as vagal nerve stimulation (VNS). Additionally, the CT images in some of the patients with iEEG monitoring might not be available, which consequently, makes it impossible for us to extract exact electrode locations for these patients. A similar situation can happen for the post-op MRI of patients undergoing surgical resection; it depends on the patient's choice if she/he would return for a post-op scan (the only way to obtain post-op MRI images). Naturally, patients with better surgical outcome are less likely to come back for another screening. These practical issues limit the number of patients who undergo resection and iEEG monitoring and at the same time their CT and post-op MRI images are available to us, as depicted in Fig. S1.

To conclude, with 39 patients of partial seizures (20 had invasive iEEG available, 34 had surgical resection outcome, and 28 had post-op MRI), we are aiming to quantitatively evaluate the capability of ictal source imaging in clinical settings in a relatively large group of patients. The detailed patient information is provided at the end of this document.

Data Acquisition

Each patient underwent long-term video EEG monitoring using a 76-channel system (XLTEK, Natus Medical Incorporated, CA, USA). A total number of 76 individual electrodes were attached to the scalp according to the 10-10 montage. The EEG signals were recorded with a 500-Hz sampling rate. The dense-array EEG was continuously recorded as conventional long-term video EEG monitoring. Ictal scalp recordings were obtained in all 39 patients. All patients

underwent an anatomical MRI scan as part of their pre-surgical evaluation. Anatomical MRI scans obtained 3-4 months post-operatively were available in some of the patients who underwent surgical resection. These scans were later used to determine the boundaries of the surgical resection. The subset of patients who underwent intracranial EEG motoring had CT images which were used to determine the location of the implanted electrodes.

Dynamic Seizure Imaging

The EEG wave forms were visually reviewed by board-certified epileptologists. The onset of seizures in EEG recordings were identified. For each seizure, we segmented the ictal epoch with a short preictal period (15-30 seconds).

The details of the proposed source analysis technique and the EEG inverse problem are discussed in detail in the following. The method is termed dynamic seizure imaging (DSI) and it is capable of imaging dynamic ictal activity from non-invasive electromagnetic surface measurements such as EEG (or MEG if ictal recordings can be obtained). The details of the frequency-domain based source imaging method, used for comparison to the DSI algorithm, are also discussed here (Fig. S2).

Source separation in Dynamic Seizure Imaging

Segments of seizure EEG (Y) of the same patient were concatenated and submitted to independent component analysis (ICA)[1–4]. The ICA separated the spatiotemporal EEG signals into N Independent components (ICs):

$$\mathbf{Y} = \sum_{i=1}^{N} \mathbf{S}_i \mathbf{T}_i \qquad (1)$$

where S_i is the scalp map of an IC indicating the fingerprint of that particular of the IC on the scalp voltage maps, and T_i is the time course of an IC indicating the temporal dynamics of the IC.

Component Selection

The ICs were selected based on the similarity between their spectrogram and the spectrogram of original EEG signal[5], because the dynamic signal change in the time and frequency domains can be observed in both IC time courses[2–4] and the scalp EEG signals. The EEG signals can be de-noised by removing the artifactual components and back-projecting the signals to EEG time courses. From the ICA analysis, the ICs with artifactual origins, such as eye blinks, eye movements and muscle activity, were rejected[4,6,7]. From the de-noised EEG signals, we computed the spectrogram of each channel using a 1-s sliding window and 50% overlap. We picked the 15 channels with the largest spectral power in the frequency band of the ictal rhythm. We then selected a subset of these 15 channels whose spectral power after the seizure onset was statistically significantly stronger than that prior to the seizure onset. The mean spectrogram of these selected channels was considered as the spectrogram of EEG (EEG-spectrogram). A spectrogram was then computed for each IC (IC-spectrogram). The statistical significance of the correlation between the EEG-spectrogram and each IC-spectrogram was tested through a nonparametric surrogate method[5,8,9]. Components significantly correlated with the time-spectral features of ictal EEG rhythms were selected as seizure components. Visual inspection was also used to assist the component selection.

Spatiotemporal Source Reconstruction

Source estimation was performed for each seizure component using a sLORETA source imaging algorithm[10]. A boundary element model (BEM) with three layers of skin, skull, and brain was used to model the head volume conductor[11–13]. A 3-dimension source model with current dipoles distributed within the brain volume was used to model the source distribution. For each seizure, the source maps, which are the IC scalp maps back-projected to the brain volume, and the corresponding IC time courses were recombined in the source domain, which

provides an approximation $\hat{Y}$ to the spatiotemporal brain activity during seizures. $L^{\dagger}$represents the lead-field matrix derived from BEM model. A few examples of reconstructed source activity can be found in Supplementary Movie S1-S3.

$$\hat{\mathbf{Y}} \approx \sum_{\mathbf{i=1}}^{\mathbf{N}} (\mathbf{L}^{\dagger}\mathbf{S_i}) \times \mathbf{T_i} \quad (2)$$

DSI Compared with a Frequency-domain Method

We compared the DSI source imaging results with another frequency-domain method[14,15], which transforms the windowed time course into Fourier space and uses the dominant ictal frequency to estimate the source distribution.

In this frequency-domain method, the original EEG signal was preprocessed to remove the eye-blink artifacts by removing the corresponding independent components. A 1-s seizure EEG was segmented at the seizure onset time interval and submitted to fast Fourier transform (FFT). The dominant ictal frequency was identified as the frequency with the maximum spectral power. For each channel of EEG, the output of FFT at the dominant frequency is a complex number with a real part and an imaginary part. In the frequency domain, the real parts of all the channels can be treated like a scalp map, and by solving an inverse problem, a source distribution of the real part can be obtained. Similarly, a source distribution of the imaginary part can also be obtained. At this point, each voxel in the source space can be represented by a complex number, where the real part and the imaginary part are estimated from the inverse problems. The source distribution of the dominant frequency can be reconstructed in the source domain by combining the real part and imaginary part of each voxel. This frequency-domain method estimates source activity using original EEG data. It estimates all the brain activity at the frequency of interest, whereas DSI extracts and estimates brain activity with time-frequency features of interest.

Extracting the dominant frequency band for seizures is a commonly used method when estimating the source of seizure activities; this however can be a source of error as the frequency of interest may be affected by artifacts. DSI, on the other hand, can separate ictal components from artifacts, noise and other background brain oscillations, thus enhancing the estimation of sources.

Source Imaging and the Number of Scalp Sensors

We then compared the source imaging results using different number of scalp electrodes. In order to achieve a virtual low-density recording, we down-sampled the IC scalp maps from 76 channels to 32 and 19 channels. We conducted the source imaging in each case, and derived DSI results for low-density configurations. Localization error was computed and compared in different sensor configurations. Note here that the down-sampling occurred while solving the inverse problem. We still used the full EEG information for ICA.

Interictal Epileptic Discharges Analysis

The extracted IEDs were classified according to the duration, the morphology, and the topology maps at IED peak. At least 5 IEDs were required to form a cluster. If more than 90% of the IEDs were in the same cluster, then only the dominant cluster was included. Otherwise all the formed clusters were included for subsequent analysis. After obtaining clustered IEDs for all patients, IEDs in the same cluster were averaged to increase the signal-to-noise ratio (SNR). sLORETA[16] was applied on the peak of the averaged IED for each IED cluster (to be consistent and in line with Dynamic Seizure Imaging algorithm as mentioned in the previous section). Two researchers had to agree on the classification and localization of the interictal findings.

Note that all the IEDs in the same cluster were averaged before source imaging analysis, which is a common practice to increase signal-to-noise ratio to ultimately improve accuracy. While using averaged IED for source imaging analysis is a common practice, there are also some

concerns about the variability of IEDs and the possible cancellation of signals caused by averaging[17]. The localization errors from IED analysis might be partially explained by the averaging process, but this is not the main focus of this study and can hardly affect the conclusions as the clustering algorithm groups spikes that are alike together, minimizing the possibility of signal cancellation due to different spikes being averaged together. Both half-rising and peak are commonly used when performing IED analysis. The half-rising point was previously proposed to accurately localize the actual "peak" in the case of spike propagation as shown in a few patients[18], whereas the peak usually has higher signal to noise ratio (SNR). In our presented work, we chose peak for IED analysis mainly for two reasons: i) we defined that the IEDs are averaged aligned to the peak to decrease potential jittering, thus the peak had the highest SNR; ii) previous publications using the same (76-channel) montage showed a relatively better localization error on the peak[19].

Evaluation Metrics

Sub-lobar Concordance

To qualitatively evaluate the performance of our analysis, we manually divided the brain into 20 cortical regions by anatomical landmarks, such as the central sulcus, the Sylvian fissure and the parieto-occipital sulcus, based on the literature[20] and adapted from prior practice[21,22]. The details regarding cortical regions division are discussed in the following.

Temporal lobe was divided into mesial temporal region, and a lateral temporal area (2 regions in each hemisphere). Frontal lobe was divided into a fronto-orbital region and the inferior, middle and superior frontal gyri (4 regions in each hemisphere). The inter-hemispheric region was maintained as one region (1 region in each hemisphere). The central region was maintained as one area (1 region in each hemisphere). The parietal lobe was maintained as one area (1 region in each hemisphere). The occipital lobe was maintained as one region (1 region in each hemisphere).

If the maximum of estimated source (in either ictal analysis or interictal analysis) and the clinical verification falls in the same cortical region, as defined above, the analysis result is defined as sub-lobar concordant.

Ictal vs Interictal Activity Comparison

Since for each patient, more than one Irritative Zone could be found (due to the existence of multiple IED clusters in some patients), the ictal activity analysis and interictal analysis were compared as following:

Qualitative Analysis Comparison

For interictal analysis, only the Irritative Zone from the Major Cluster was included for qualitative analysis. The interictal and ictal analysis were compared in five groups: all patients, the patients with ILAE1-2 outcome, the patients with ILAE3-5 outcome, the patients with only 1 cluster, and the patients with more than 1 clusters.

Quantitative Analysis Comparison

The quantitative results from interictal analysis were rearranged into three groups:

- All clusters: localization error from all the clusters among all patients were included, which means the total number of LEs were more than the number of patients in this data group and equal to the number of clusters (n=59).
- Major cluster: for each patient, the cluster with most IEDs will be considered as the Major Cluster. Each patient had only one interictal analysis result in this group of data.
- Closest cluster: for each patient, the cluster with smallest LE was considered as the Closest Cluster. Each patient had only one interictal analysis result in this group of data.

Each group were then compared to the ictal analysis results.

Shuffling Process

One concern about the previous comparisons is with respect to the Major Cluster definition. In pre-surgical diagnosis process, clinicians tend to use other sources of information (MRI, semiology, PET, SPECT, etc.) to determine the relevance of IEDs in determining the epileptogenic zone, and they may or may not reach a consensus. Also, the method we used previously (considering the cluster with the highest number of IEDs as the Major Cluster) may not be the same as clinical consensus[23], as we only consider the inter-ictal IEDs with barely any other clinically relevant information. Thus, if multiple IED clusters exist, there would be a chance for each cluster to be considered as the relevant IED. Given all the other relevant clinical data that our approach is agnostic of, and solely basing our results on electrophysiological recordings, the detected IED numbers in each cluster might bias our analysis results as IEDs might have been missed when EEG recordings were inspected, which subsequently changes the IED numbers in each cluster which might have resulted in another cluster to have been selected as the Major Cluster, which could ultimately affect the clinical diagnosis.

To fully address this potential issue of interictal analysis, first we defined the interictal analysis result from Major Cluster, i.e. the localization error, to be a weighted average of LEs from all the clusters. For example, in Major Cluster group as defined above, the weighting will be 1 for the cluster with most IEDs, and 0 for others. In the shuffling process, the weighting for each cluster detected for each patient, would be randomly generated to have a value between 0 and 1, while the sum of weighting for each patient would equal 1. After each shuffle, we compared the ictal analysis LE with the weighted interictal analysis LE and a P value was calculated. By performing this process, we compared the overall sensitivity of interictal analysis performance with ictal analysis performance. This weighting process, in some degree, represents a decision-making process where information from each IED cluster plays a role in determining the relevant epileptic region. The results depicted in Fig. S3 indicate that the majority of these comparisons resulted in significant p-values, as evident by the skew of the distribution to the left, validating the robustness of using the Major cluster for comparing IED analysis results to ictal analysis results.

ILAE Classification Scales of Post-operative Outcome

Class 1:	Completely seizure free since surgery; no aura
Class 2:	Only auras; no other seizures
Class 3:	1 to 3 seizure days per year; ± auras
Class 4:	4 seizure days per year to 50% reduction of baseline seizure days; ± auras
Class 5:	Less than 100% reduction of baseline seizure days; ± auras
Class 6:	More than 100% increase of baseline seizure days; ± auras

Patient Exclusion and Explanation

We computed the localization error as the minimum distance between the estimated source maximum to all the electrodes involved in the iEEG-SOZ. For all 20 patients that underwent iEEG recording, the mean localization error was about 2.0 cm. However, there were two cases in which the DSI identified sources at regions without iEEG coverage. By removing these two cases, the mean localization error is approximately 1.35 cm.

In one case, the iEEG of one patient recorded the seizure onset by the left temporal strips and depth electrodes (Movie S4 blue electrodes). Whereas from the scalp EEG, seizures of the patient started from generalized areas with the estimated source maximum in the midline of the brain, shortly after which the seizures propagated to and became significant at the left temporal lobe (Movie S4). The patient was not seizure free and an ILAE-4 outcome was reported for this patient, at the most recent follow-up. The DSI results suggest more iEEG coverage in the midline of the brain may have been beneficial for pre-surgical planning.

In the second case, the DSI identified source in the lateral left temporal lobe, whereas iEEG measured seizure onset by right temporal depth electrodes. Only depth electrodes were implanted in this patient, and therefore other areas of the brain were poorly sampled. After surgery, the patient was not seizure free as reported by the most recent follow-up.

We also want to provide potential explanations for such observed discrepancy. For the first case as shown in Fig. S4a, clinically, scalp EEG showed frequent epileptiform discharges arising from the left and right frontotemporal head regions, maximal left. During the recording, the patient's typical seizure appeared to be of left frontotemporal onset. The DSI localization results of the patient also showed that the activities started from generalized areas with the estimated source maximum in the frontal midline of the brain, shortly after which the seizures propagated to and became significant at the left temporal lobe. Based on the initial assessments, the clinicians decide to implant the intracranial electrodes (strips, grids, and depth electrodes) over the left temporal and frontal region. Limited by the techniques back in 2009, most of the electrodes didn't go too deep, thus, the SOZ identified were the left temporal depth electrodes and mesial contacts of the sub-temporal strips.

In the second case as presented in Fig. S4b, scalp EEG showed frequent epileptiform discharges and slowing over both temporal regions during wakefulness and sleep. During the recording, the patient's typical complex partial seizures were indeterminate as to localization and showed features that would support left and right lateralization. The ictal EEG was most consistent with left temporal onset seizures. The DSI also showed maximum activation pattern on the left temporal lobe for the EEG onset. Based on the initial assessments, intraoperative electrocorticography was performed using bilateral temporal 8-contact depth electrodes within the hippocampus and oriented parallel to its axis from a posterior approach. All clinical seizures demonstrated right temporal depth electrode onset with spread to the left temporal depth electrodes thus right temporal lobectomy and amygdalohippocampectomy were performed.

In these two cases, we can infer that the discrepancy is not between the clinical scalp EEG signal and the DSI results (i.e. DSI results not fitting EEG measurements), but more likely between DSI results and the intracranial electrodes placement based on clinical assessments and placement hypotheses. While intracranial electrodes can directly record the cortical/subcortical activities, they also suffer from poor spatial sampling. From Fig. S4, it is clear that the seizure onset identified using DSI was not covered by the intracranial electrodes. There are several recent studies showing that the scalp EEG/MEG can provide added value to intracranial studies, especially in the case of sparse sampling[24,25].

To emphasize this point again, although in those two cases with poor DSI localization results, the surgical outcome is not ideal and the regions identified from DSI were not covered by iEEG electrodes, we are not suggesting that the DSI results would be the "true" epileptogenic zone due to limited data and the retrospective nature of this study. However, with the advanced understanding that epilepsy is a network disease[26], different onset sites provided by various imaging modalities, such as DSI on high-density scalp EEG, can be considered as nodes constructing the epileptic network and thus play an assistive role in the presurgical evaluation.

Ictal pattern and DSI performance

From the clinical reports, we summarized the electrographic patterns of the 37 patients (as summarized in Patient Information Section, Table S5) in both scalp EEG and intracranial EEG (if available). The two patients with very large LE were not included, following our methodology.

For scalp EEG, we categorized them based on the description from clinical reports and the categories are: i) alpha; ii) beta; iii) fast activity; iv) theta; v) theta/alpha; vi) theta/delta; vii) delta; viii) slow wave; ix) poly spike; x) sharp wave. In Fig. S5a and S5b, we showed the boxplot for LEs in each category. However, since there are 10 categories, the number of patients in each category can be small.

To visualize the data better, we re-grouped the 10 categories as follow: alpha → alpha; beta, fast activity → beta; theta, theta/alpha → theta; delta, slow wave, theta/delta → delta; poly spike, sharp wave → others. With the reorganized groups, the LEs are represented in Fig. S5c and S5d. Fig. S5e and S5f show the results in seizure-free patients.

For intracranial EEG, we followed the criteria in literature[27], and used the criteria on the available intracranial EEG reports. The categories we found are: i) burst-suppression; ii) delta; iii) fast activity; iv) poly-spike; v) sharp activity; vi) spike and wave activity. In Fig. S6, we showed the boxplot for LEs in each category.

From Fig. S5 and S6, it can be inferred that the scalp EEG onset patterns may have influenced the localization error. In Fig. S5c and S5E, as the frequency range for the onset pattern increases, the localization error seems to increase as well. Especially in Fig. S5c, we ran Wilcoxon-rank-sum test on LEs for delta and theta (N=5), vs LEs for alpha and beta (N=9), and the difference is marginally significant (p=0.042). This might be explained by higher energy/amplitude in lower-frequency oscillations, which enhanced SNR for better localization accuracy. However, due to limited number of patients in each category (especially for seizure-free cases), whether the effect will hold, in general, still deserves further investigation.

It is also interesting to note that the initial onset patterns in scalp EEG are not exactly like the initial onset patterns in intracranial EEG (as shown in Table S5). There could be multiple explanations. For example, some intracranial EEG patterns may not be detected on scalp EEG as scalp recordings might not capture early ictal onset signals. We also found literature in support of our findings[28]. Simultaneous EEG and iEEG recording are ideal to address this issue, but such recordings are also difficult to perform over long-enough periods to capture enough seizures in a large group of patients.

SUPPLEMENTARY TABLES

Table S1. Localization error (LE) Comparison among Different Montages (Two-sided t-test)

Localization Error Comparison	Patients with iEEG	Patients with Surgical Resection	Patients with Seizure-free Lobectomy Outcome
76 vs 32	P = 0.04616	P = 0.4166	P = 0.2117
32 vs 19	P = 0.04929	P = 0.01067	P = 0.02805
76 vs 19	P = 0.001693	P = 0.001232	P = 0.004593

Table S2. Ictal and Interictal Localization error (LE) Comparison for Patients with iEEG (Two-sided Wilcoxon Rank Sum Test)

LE Comparison (Wilcoxon Rank Sum Test)	All Patients	ILAE1-2 Patients	ILAE3-5 Patients
Ictal vs All Clusters	P = 0.0004851	P = 0.1614	P = 0.002664
Ictal vs Major Cluster	P = 0.00788	P = 0.3357	P = 0.03175
Ictal vs Closest Cluster	P = 0.07274	P = 0.8665	P = 0.03175

Table S3. Ictal and Interictal Localization error (LE) Comparison for Patients with Surgical Resection (Two-sided Wilcoxon Rank Sum Test)

LE Comparison (Wilcoxon Rank Sum Test)	All Patients	ILAE1-2 Patients	ILAE3-5 Patients
Ictal vs All Clusters	P = 0.7629	P = 0.6067	P = 0.8523

SUPPLEMENTARY FIGURES

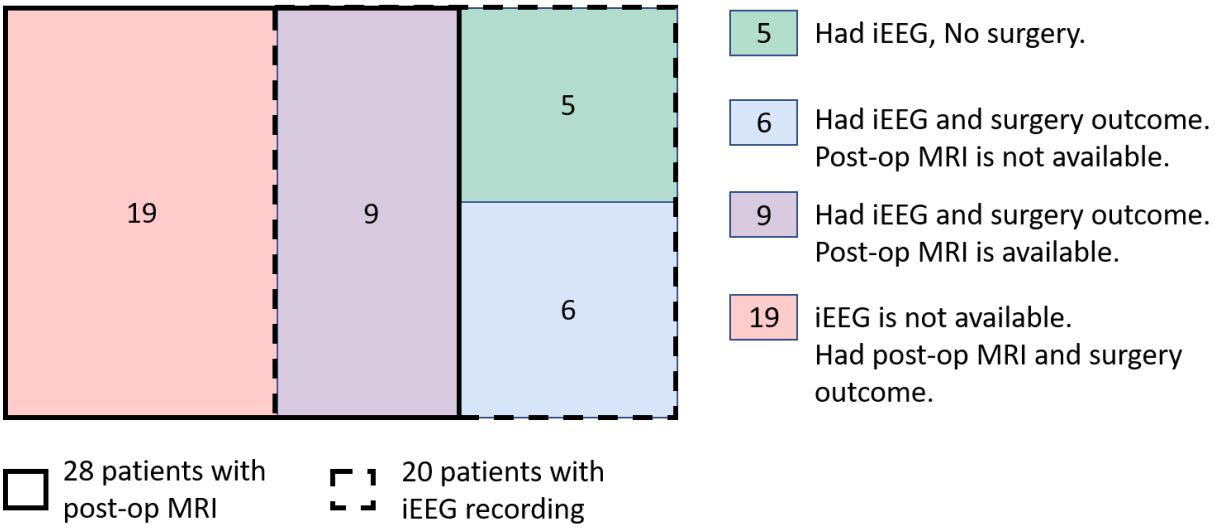

Fig. S1. The Patient Number Breakdown

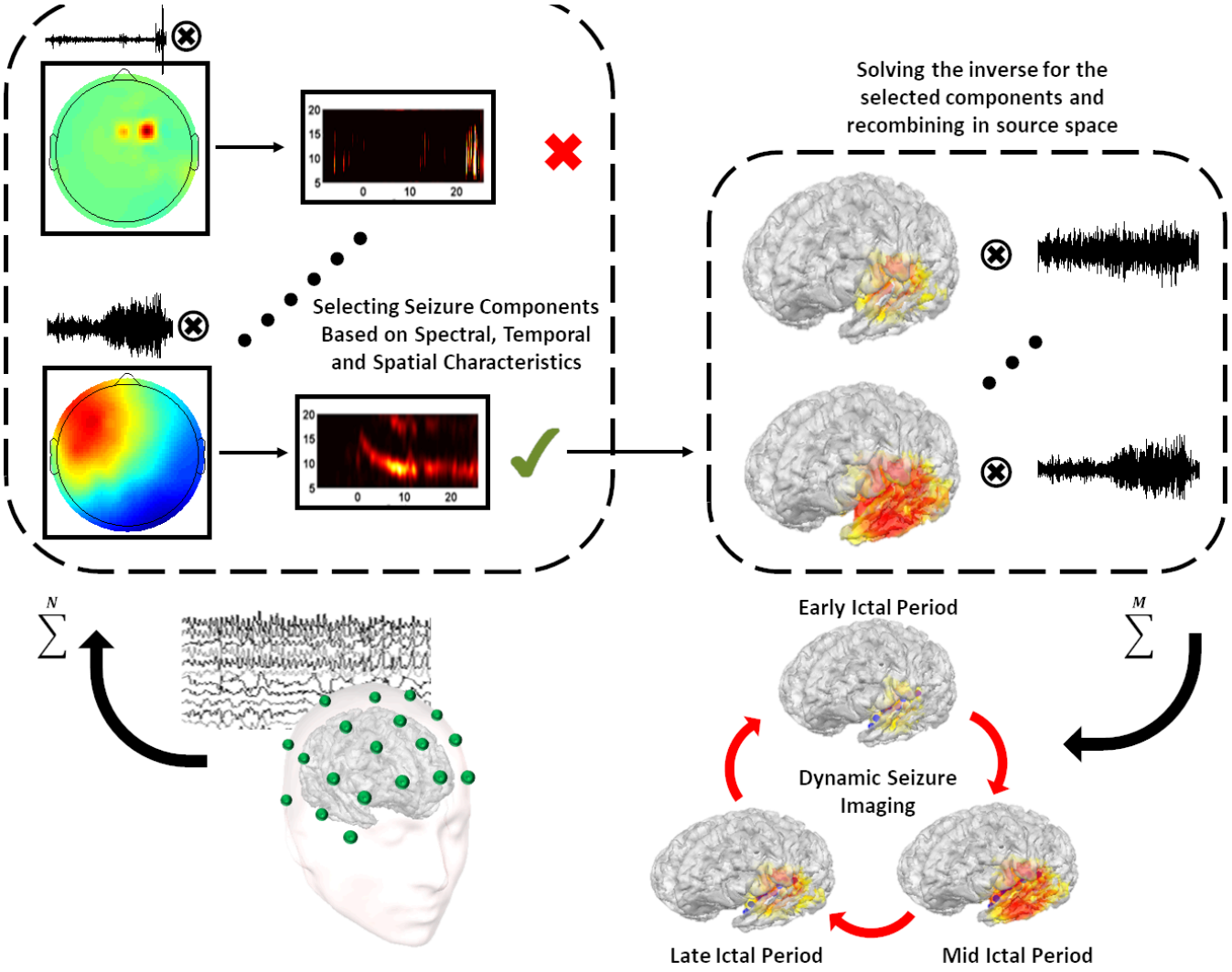

Fig. S2. The flowchart of the dynamic seizure imaging (DSI) algorithm. It involves steps of independent component analysis (**ICA**), solving the inverse problem, and source re-combination.

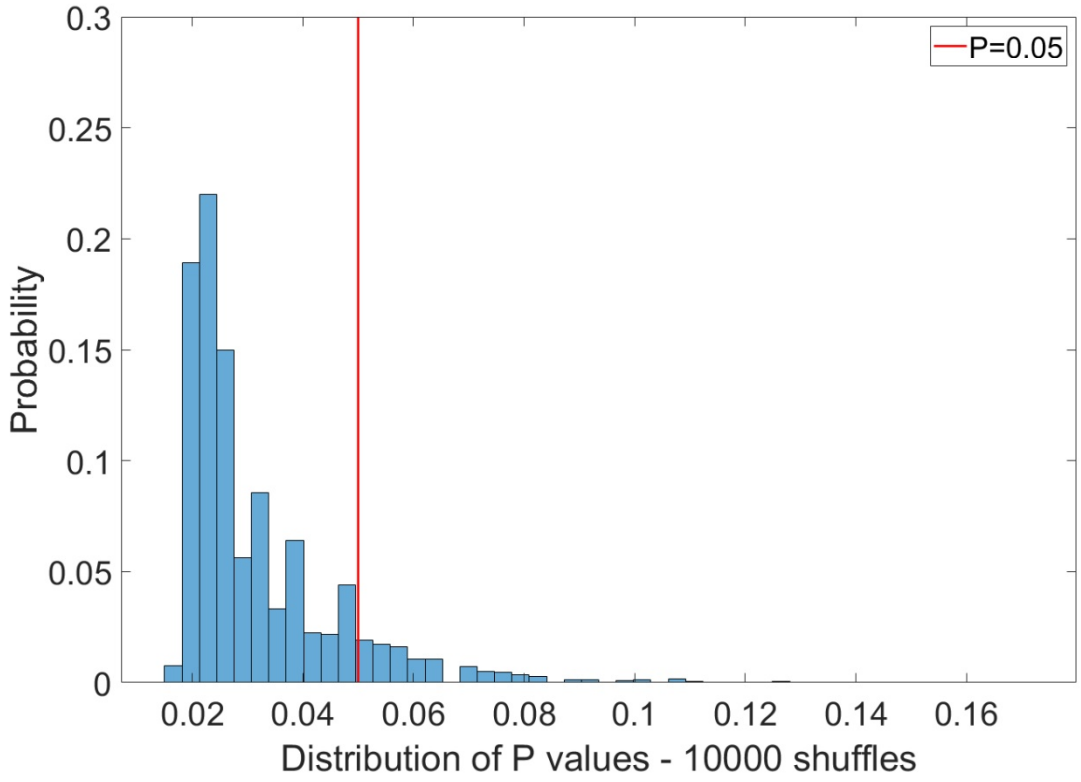

Fig. S3. P-values distribution by comparing shuffled interictal results with ictal analysis results. We defined the localization error to be a weighted average of the all the clusters, while the weighting would be randomly shuffled. In each shuffle, we compared the ictal analysis LE with the weighted interictal analysis LE and a P-value was calculated. After 10,000 shuffles, the distribution of P values showed that in majority of the cases, ictal analysis still maintained a significantly better performance than interictal analysis.

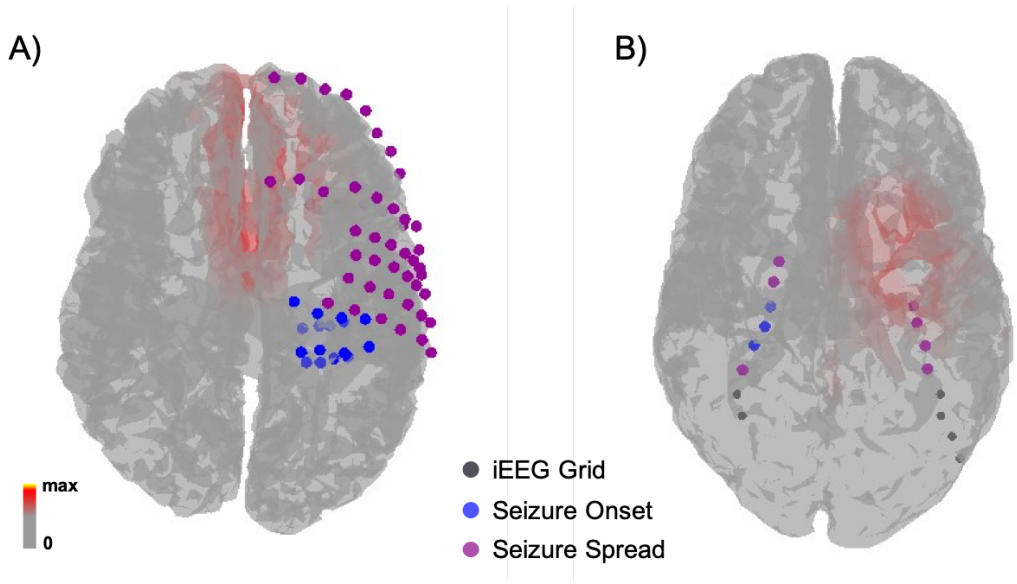

Fig. S4. The bottom view of the two cases with large localization errors. DSI results showed by the red activation patterns are overlaid with the iEEG electrodes showing the clinically-identified SOZ. Blue electrodes are the seizure onset electrodes. Purple electrodes are the seizure spread electrodes. Grey electrodes are the ones without seizure activities.

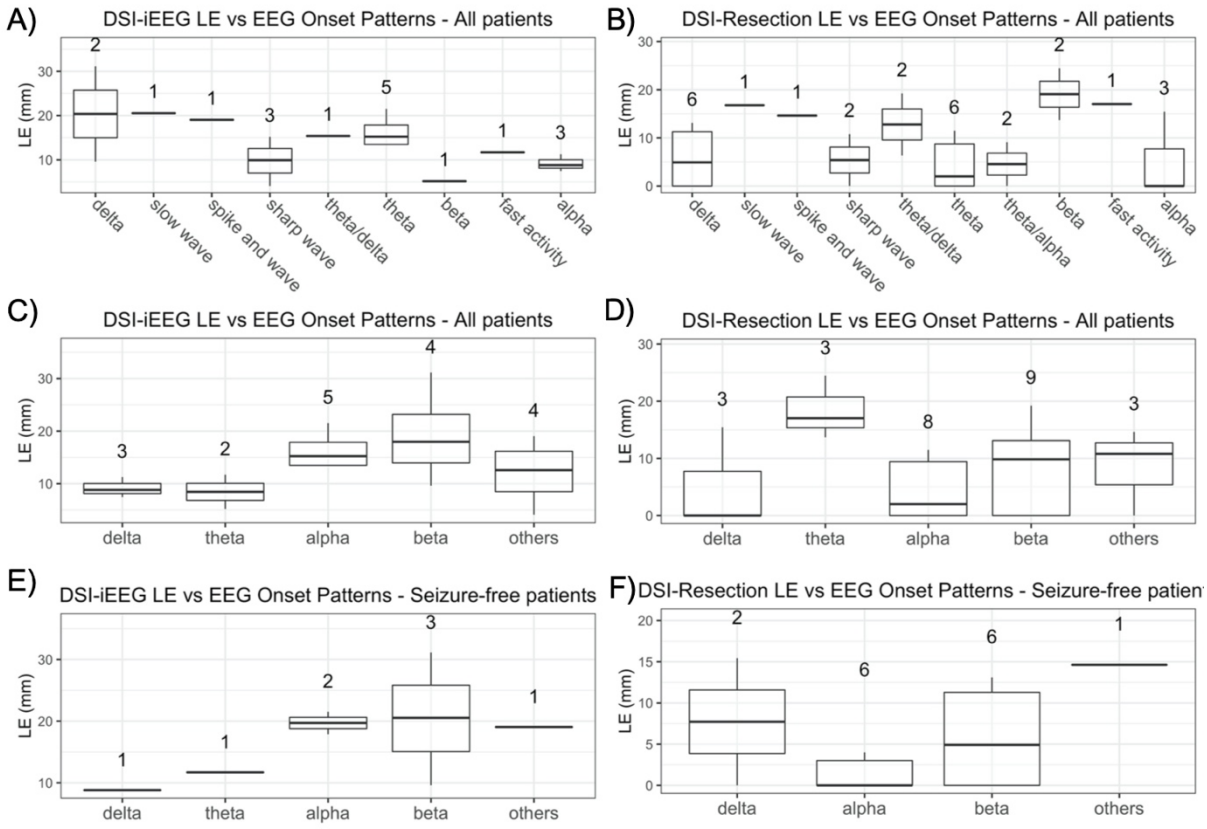

Fig. S5. The boxplot of LEs in categories based on scalp EEG onset patterns. A) all patients' LEs (comparing to iEEG-SOZ) with 10 initial categories; B) all patients' LEs (comparing to resection) with 10 initial categories; C) all patients' LEs (comparing to iEEG-SOZ) with 5 re-grouped categories; D) all patients' LEs (comparing to resection) with 5 re-grouped categories; E) seizure-free patients' LEs (comparing to iEEG-SOZ) with 5 re-grouped categories; F) seizure-free patients' LEs (comparing to resection) with 5 re-grouped categories.

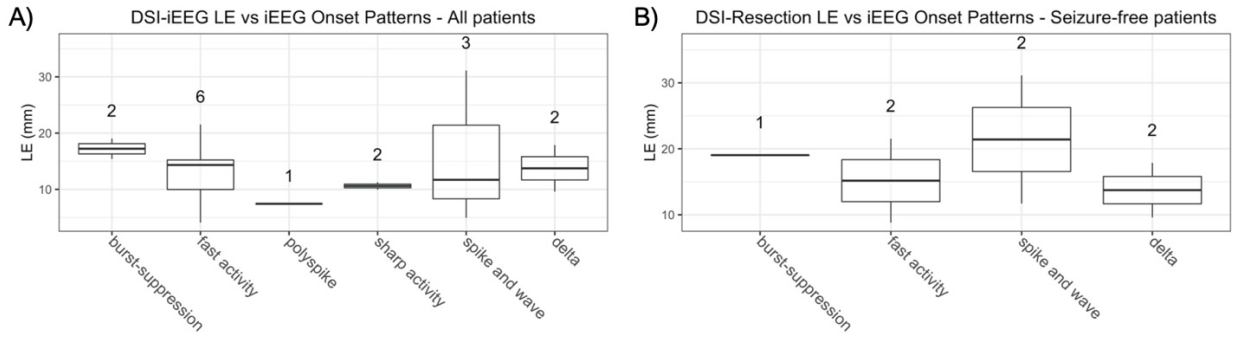

Fig. S6. The boxplot of LEs in categories based on iEEG onset patterns. A) all patients' LEs (comparing to iEEG-SOZ) with 6 categories; B) seizure-free patients' LEs (comparing to iEEG-SOZ) with 6 categories.

SUPPLEMENTARY MOVIE CAPTIONS

Movie S1. Spatiotemporal imaging of a seizure in one patient with depth electrodes. The seizure started from the left temporal lobe and remained in the left hemisphere without propagating to other regions, as indicated by both EEG source imaging and iEEG.

Movie S2. Spatiotemporal imaging of a seizure in one patient with iEEG electrodes. The seizure started from the right posterior temporal lobe and remained in the right hemisphere without propagation, as indicated by both EEG source imaging and iEEG.

Movie S3. Spatiotemporal imaging of a seizure in one patient with parietal lobe onset. The seizure started from the right parietal region with fast propagation to the right temporal region. Both regions were covered with iEEG electrodes and were indicated as seizure onset zones by EEG source imaging and iEEG.

Movie S4 Spatiotemporal imaging of a seizure in one patient with limited iEEG electrodes coverage. Dynamic seizure imaging shows the seizure started from generalized areas of the brain with maximal activity in the midline of the brain. Shortly after, the seizure became strongest in the left temporal lobe. The iEEG covers only limited regions of the brain and therefore cannot provide information regarding the brain activity in regions indicated by non-invasive source imaging. The patient was not seizure-free post-surgery.

PATIENT INFORMATION

Table S4. Patient Information

Index	**Age at Surgery**	**Gender**	**MRI Assessment**	**Intracranial SOZ**	**Surgery**	**Outcome**	**Duration of Follow Up**
1	33	Female	Normal	Right temporal grids and strips and depth electrodes on mesial side	Right anterior temporal lobectomy and amygdalohippocampectomy	ILAE-1	1 year
2	21	Female	Normal	Right temporal grids and strips and depth electrodes on mesial side	Right anterior temporal lobectomy and amygdalohippocampectomy	ILAE-1	1 year
3	N.A.	Female	Normal	Left frontal and temporal grids and strips and mesial depth electrodes	Left anterior temporal lobectomy and amygdalohippocampectomy	ILAE-2	1 year
4	N.A.	Female	Normal	Right temporal grids and strips and depth electrodes on mesial side	Right temporal lobectomy and amygdalohippocampectomy	ILAE-1	1 year
5	60	Female	Left, mesiotemporal atrophy	N.A.	Left temporal lobectomy and amygdalohippocampecomy	ILAE-1	32 months
6	45	Male	Right, chronic MCA infarct	Right frontotemporal parietal grid electrodes	Frontal temporal lobectomy	ILAE-1	1 year
7	53	Female	General cerebral atrophy	Right temporal grids and strips and depth electrodes on mesial side	Left temporal lobectomy and amygdalohippocampecomy	ILAE-1	1 year
8	25	Female	Normal	Right temporal grids and strips and depth electrodes on mesial side	Right temporal lobectomy and amygdalohippocampectomy	ILAE-1	1 year
9	38	Male	Normal	Multiple right lateral temporal and sub-temporal grids and strips of electrodes	Extended right temporal lobectomy with amygdalohippocampectomy	ILAE-1	15 months

10	48	Male	Right hippocampal atrophy	Right temporal grids and strips and depth electrodes on mesial side	Right temporal lobectomy and amygdalohippocampectomy	ILAE-1	1.5 years
11	51	Female	Right, lesion	Right temporal grids and strips and depth electrodes on mesial side	Right anterior temporal lobectomy and amygdalohippocampectomy	ILAE-1	1 year
12	25	Female	Normal	Left frontal, pariental, temporal and occipital grids and strips of electrodes	Left parietal focal cortical resection	ILAE-1	1 year
13	19	Female	Left, temporal hematoma	N.A.	Left temporal excision; residual left temporal cavernous hemangioma	ILAE-1	20 months
14	21	Male	Left, encephalomalacia	Left frontal strips	Modified left frontal lobectomy	ILAE-1	19 months
15	49	Male	Right, cavernous malformation	N.A.	Right temporal lesion resection	ILAE-1	20 months
16	15	Female	Normal	Multiple stereo EEG electrodes	Right frontal	ILAE-1	19 months
17	22	Female	Left, mesial temporal sclerosis	Left frontotemporal subdural grid, strip and depth electrodes	Left anterior temporal lobectomy. Amygdalohippocampectomy.	ILAE-1	14 months
18	25	Male	Normal	Multiple stereo EEG electrodes	Stereotactic excision, right mesial frontal orbital lobe	ILAE-2	1 year
19	25	Male	Right, subjacent brain encephalomalacic	Right temporoparietal and right parietal grid, right temporal depth electrodes	Right frontotemporal lobe resection	ILAE-5	1 year
20	39	Male	Normal	Bitemporal depth electrodes	Right temporal lobectomy and amygdalohippocampectomy	ILAE-4	13 months
21	50	Female	Right, mesial temporal sclerosis	Right temporal strips and mesial temporal depth electrodes	Right temporal lobectomy and amygdalohippocampectomy	ILAE-3	19 months
22	29	Male	Bilateral mesial temporal sclerosis	Right temporal strips and mesial temporal depth electrodes	Right anterior temporal lobectomyand amygdalohippocampectomy	ILAE-4	18 months

23	22	Female	Normal	Left temporal grid and strips on the inferior temporal side and left frontal, depth electrodes on temporal and frontal	Left anterior temporal lobectomy and amygdalohippocampectomy	ILAE-3	1 year
24	22	Female	Normal	Right fronto-temporal grids and strips and depth electrodes close to amygdala and hippocampus, and later right posterotemporo-parietal grids and strips	Focal temporo-occipital cortical resection	ILAE-4	12 months
25	29	Male	Normal	Right temporal strips	Right temporal lobectomy and amygdalohippocampectomy	ILAE-4	13 months
26	58	Female	Left, mild cerebral and cerebellar atrophy	left temporal strips and mesial depth electrodes	Left temporal lobectomy and amygdalohippocampectomy	ILAE-4	15 months
27	N.A.	Female	Left, mesial temporal sclerosis	Left temporal strips and electrodes	Left anterior temporal lobectomy and amygdalohippocampectomy	ILAE-3	12 months
28	34	Male	Normal	Left temporal grids and strips and depth electrodes	Resection of lateral temporal neocortex extending into parietal cortex	ILAE-6	22 months
29	37	Male	Right hemispheric atrophy and left hippocampal atrophy	Right frontotemporal grid strips and depth electrodes.	Right frontal	ILAE-4	13 months
30	47	Male	Left, mesial temporal sclerosis	Left temporal subdural grid, strip electrodes, and left depth electrodes	Left anterior temporal lobectomy and amygdalohippocampectomy. Left posterior temporo-occipital corticectomy.	ILAE-3	21 months
31	17	Male	Right, focal cortical dysplasia	N.A.	Laser ablation of RIGHT frontal malformation of cortical development.	ILAE-3	1 year

32	39	Male	Left, mesial temporal sclerosis	N.A.	Laser ablation of LEFT mesial temporal sclerosis.	ILAE-1	1 year
33	13	Male	Left, focal cortical dysplasia	Multiple stereo EEG electrodes	Laser interstitial thermotherapy of the Visualase tract (VT)	ILAE-1	1 year
34	52	Female	Left, focal atrophy	NA	Laser ablation of left amygdala hippocampus.	ILAE-1	18 months
35	46	Male	Left, punctate	Bitemporal depth electrode	N.A.	No surgery	N.A.
36	26	Female	Normal	left hemisphere strips, grids, and depth electrodes	N.A.	No surgery	N.A.
37	39	Male	Bilateral hippocampi atrophy	Bitemporal depth electrodes	N.A.	No surgery	N.A.
38	20	Female	N.A.	Right hemisphere strips and grids, and double-sided interhemispheric strips	N.A.	No surgery	N.A.
39	25	Male	Normal	Subdural strips and grid electrodes over the right frontal and right interhemispheric frontal region	N.A.	No surgery	N.A.

Table S5. Patient EEG and iEEG Onset Patterns

Index*	EEG onset patterns as in clinical reports	Category	iEEG onset pattern	iEEG Category
1	rhythmic delta activity	delta		
2	rhythmic delta slowing	delta		
3	rhythmic delta slowing	delta	a rhythmic spike and wave discharge	spike and wave
4	rhythmic delta slowing	delta		
5	rhythmic 4 Hz theta frequency discharge	theta		
6	rhythmic theta slowing	theta	rhythmic delta activity	delta
7	a sharp wave followed by rhythmic theta activity	theta		
8	theta or alpha frequency activity	theta/alpha		
9	rhythmic theta frequency discharge	theta	a fast frequency discharge	fast activity
10	rhythmic alpha discharge	alpha	a fast activity	fast activity
11	rhythmic delta sharp wave	delta		
12	polyspike and wave discharge	spike and wave	a sentinel sharp wave followed by generalized attenuation and low voltage paroxysmal fast activity	burst-suppression
13	rhythmic delta	delta		
14	a brief alpha frequency discharge evolved into low amplitude fast activity	alpha		
15	a prominent theta alpha rhythm	theta/alpha		
16	fast activity evolved to rhythmic delta	fast activity	spike-wave discharges	spike and wave
17	rhythmic delta activity	delta	initial rhythmic delta activity with overlying fast activity	delta
18	slow wave discharge	slow wave	* Didn't specify	

19	low amplitude repetitive sharp wave discharges	sharp wave	rhythmic spikes of fast frequency and then evolved to a rhythmic delta in surrounding	fast activity
20	rhythmic delta slowing	delta	sharp waves firing at a frequency of about 1 Hz in right temporal depth electrodes	sharp activity
21	a theta frequency discharge	theta		
22	a rhythmic theta frequency discharge	theta		
23	rhythmic intermixed theta and delta activity	theta/delta	diffuse attenuation then sharp wave	burst-suppression
24	rhythmic delta and theta frequency activity	theta/delta	a spike discharge followed by generalized attenuation	burst-suppression
25	theta or delta activity	theta/delta		
26	alpha frequency activity	alpha		
27	repetitive sharp waves	sharp wave		
28	rhythmic theta range activity	theta	a brief run of spike and wave discharges	spike and wave
29	a small initial sharp wave followed by electrodecrement	sharp wave	low amplitude fast activity in the gamma/beta range	fast activity
30	initial frequent sharp wave activity evolved into rhythmic theta activity.	sharp wave	sharp contoured rhythmic activity in the alpha/beta range	sharp activity
31	initial slow waves followed by alpha	slow wave		
32	generalized attenuation with fast bifrontal beta	beta		
33	fast activity	fast activity		
34	beta frequency fast activity	beta		
35	rhythmic theta activity	theta	increasing high frequency spikes	fast activity
36	rhythmic alpha discharges	alpha	a brief polyspike discharge	polyspike
37	rhythmic 4 Hz theta frequency discharge	theta	low amplitude fast activity and a gamma frequency discharge	fast activity
38	rhythmic alpha frequency discharge	alpha	an alpha frequency discharge	sharp activity
39	an increased frequency in the beta range	beta	* Didn't specify	

*The index in Table S5 is not necessarily the same as in Table S4.

REFERENCES

1 Delorme A, Makeig S. EEGLAB: an open source toolbox for analysis of single-trial EEG dynamics including independent component analysis. *J Neurosci Methods* 2004; **134**: 9–21.

2 Nam H, Yim T-G, Han SK, Oh J-B, Lee SK. Independent Component Analysis of Ictal EEG in Medial Temporal Lobe Epilepsy. *Epilepsia* 2002; **43**: 160–4.

3 Patel A, Alotaibi F, Blume WT, Mirsattari SM. Independent component analysis of subdurally recorded occipital seizures. *Clin Neurophysiol* 2008; **119**: 2437–46.

4 Jung K-Y, Kang J-K, Kim JH, Im C-H, Kim KH, Jung H-K. Spatiotemporospectral characteristics of scalp ictal EEG in mesial temporal lobe epilepsy with hippocampal sclerosis. *Brain Res* 2009; **1287**: 206–19.

5 Yang L, Wilke C, Brinkmann B, Worrell GA, He B. Dynamic imaging of ictal oscillations using non-invasive high-resolution EEG. *Neuroimage* 2011; **56**: 1908–17.

6 Jung T-P, Makeig S, Humphries C, *et al.* Removing electroencephalographic artifacts by blind source separation. *Psychophysiology* 2000; **37**: 163–78.

7 Urrestarazu E, Iriarte J, Alegre M, Valencia M, Viteri C, Artieda J. Independent component analysis removing artifacts in ictal recordings. *Epilepsia* 2004; **45**: 1071–8.

8 Palus M, Hoyer D. Detecting nonlinearity and phase synchronization with surrogate data. *Eng Med Biol Mag IEEE* 1998; **17**: 40–45.

9 Theiler J, Eubank S, Longtin A, Galdrikian B, Farmer JD. Testing for nonlinearity in time series: the method of surrogate data. *Phys D Nonlinear Phenom* 1992; **58**: 77–94.

10 Wagner M, Fuchs M, Kastner J. SWARM: sLORETA-weighted accurate minimum norm inverse solutions. *Int Congr Ser* 2007; **1300**: 185–8.

11 Fuchs M, Drenckhahn R, Wischmann H, Wagner M. An improved boundary element method for realistic volume-conductor modeling. *IEEE Trans Biomed Eng* 1998; **45**: 980–997.

12 Hamalainen MS, Sarvas J. Realistic conductivity geometry model of the human head for interpretation of neuromagnetic data. *Biomed Eng IEEE Trans* 1989; **36**: 165–171.

13 He B, Musha T, Okamoto Y, Homma S, Nakajima Y, Sato T. Electric dipole tracing in the brain by means of the boundary element method and its accuracy. *Biomed Eng IEEE Trans* 1987; : 406–414.

14 Yuan H, Doud A, Gururajan A, He B. Cortical Imaging of Event-Related (de)Synchronization During Online Control of Brain-Computer Interface Using Minimum-Norm Estimates in Frequency Domain. *IEEE Trans Neural Syst Rehabil Eng* 2008; **16**: 425–31.

15 Yuan H, Liu T, Szarkowski R, Rios C, Ashe J, He B. Negative covariation between task-related responses in alpha/beta-band activity and BOLD in human sensorimotor cortex: An EEG and fMRI study of motor imagery and movements. *Neuroimage* 2010; **49**: 2596–606.

16 Pascual-Marqui RD. Standardized low resolution brain electromagnetic tomography (sLORETA): technical details. *Methods Find Exp Clin Pharmacol* 2002; **24**: 5–12.

17 Ahlfors SP, Han J, Lin FH, *et al.* Cancellation of EEG and MEG signals generated by extended and distributed sources. *Hum Brain Mapp* 2010; **31**: 140–9.

18 Lantz G, Spinelli L, Seeck M, De Peralta Menendez RG, Sottas CC, Michel CM. Propagation of Interictal Epileptiform Activity Can Lead to Erroneous Source Localizations: A 128-Channel EEG Mapping Study. *J Clin Neurophysiol* 2003. DOI:10.1097/00004691-200309000-00003.

19 Wang G, Worrell G, Yang L, Wilke C, He B. Interictal spike analysis of high-density eeg in patients with partial epilepsy. *Clin Neurophysiol* 2011; **122**: 1098–105.

20 Agirre-Arrizubieta Z, Huiskamp GJM, Ferrier CH, Van Huffelen AC, Leijten FSS. Interictal magnetoencephalography and the irritative zone in the electrocorticogram. *Brain* 2009; **132**: 3060–71.
21 Huiskamp G, Agirre-Arrizubieta Z, Leijten F. Regional differences in the sensitivity of MEG for interictal spikes in epilepsy. *Brain Topogr* 2010; **23**: 159–64.
22 Pellegrino G, Hedrich T, Chowdhury R, *et al.* Source localization of the seizure onset zone from ictal EEG/MEG data. *Hum Brain Mapp* 2016; **37**: 2528–46.
23 Bartolomei F, Trébuchon A, Bonini F, *et al.* What is the concordance between the seizure onset zone and the irritative zone? A SEEG quantified study. *Clin Neurophysiol* 2016; **127**: 1157–62.
24 Hosseini SAH, Sohrabpour A, He B. Electromagnetic source imaging using simultaneous scalp EEG and intracranial EEG: An emerging tool for interacting with pathological brain networks. *Clin Neurophysiol* 2018; **129**: 168–87.
25 Rikir E, Koessler L, Gavaret M, *et al.* Electrical source imaging in cortical malformation-related epilepsy: A prospective EEG-SEEG concordance study. *Epilepsia* 2014; **55**: 918–32.
26 Kramer MA, Cash SS. Epilepsy as a disorder of cortical network organization. *Neuroscientist* 2012; **18**: 360–72.
27 Perucca P, Dubeau F, Gotman J. Intracranial electroencephalographic seizure-onset patterns: Effect of underlying pathology. *Brain* 2014; **137**: 183–96.
28 Tanaka H, Khoo HM, Dubeau F, Gotman J. Association between scalp and intracerebral electroencephalographic seizure-onset patterns: A study in different lesional pathological substrates. *Epilepsia* 2018; **59**: 420–30.